Twelfth Australasian Fluid Mechanics Conference
The University of Sydney, Australia 1995

MEASUREMENT OF SECONDARY FLOW VELOCITY AND TURBULENCE IN A TWISTED S-TUBE

Yoshiyuki Aoyama
Department of Mechanical Engineering
Ehime University
Matsuyama
Japan

Koichi Murakami
Department of Mechanical Engineering
Ehime University
Matsuyama
Japan

ABSTRACT

The time-mean axial and secondary flow velocities and the fluctuating velocity correlations were measured in the turbulent flow through a circular-sectioned twisted S-tube using a hot wire probe. A pair of symmetric secondary-flow vortices generated in the fore bend of twisted S-tube change to become almost a single vortex in the hind bend. Turbulence intensity increases sharply near the inside wall of the hind bend by the 45-degree turn of it. The distribution of the generation rate for the turbulence intensity is correlated with that of the intensity.

INTRODUCTION

Turbulent flow through circular-section pipe bends can be seen in heat exchangers and in various pipe lines in a plant. Several papers have reported the experimental results for the distribution of the time-mean velocities and the turbulence intensities in 90-degree or 180-degree bends(Rowe, 1970; Enayet et al., 1982; Azzola et al., 1986; Aoyama et al., 1990). Iacovides and Launder(1984) and Akiyama et al.(1988) numerically solved the momentum and the heat transport equations for the flow in these bends by using a turbulence model. In addition, heat transfer measurments were also carried out by Baughn et al(1987). These studies make us aware of the characteristics of the flow field and the heat transfer in a single bent tube. It is well known, therefore, that the axial velocity profile is drastically distorted from that in a straight tube due to the secondary flow. But the characteristics for the single bend cannot be valid for a complex tube with bends. The pipe bends, in fact, are often connected complexly in a three dimensional rotation, though that case occurs less frequently than the case of the single bend utilization. There seems, however, to have been no investigation into the variation of the amount of turbulence in the flow through those complex tubes.

In this study, the time-mean axial and secondary flow velocities, and the correlations of the fluctuating velocities were measured in the turbulent flow through the twisted S-tube by using a hot wire anemometer. The twisted S-tube having a circular cross-section is composed of a pair of 90-deg bends, where the curvature plane of the hind bend was perpendicular to that of the fore bend (each bend is geometrically symmetric with respect to the curvature plane).

COMPOSITION OF THE BENDS AND COORDINATES

Figure 1 shows schematically the circular twisted S-tube composed of a pair of 90-deg bends, where the time-mean velocities and the fluctuating velocity correlations are measured. Each bend is also composed of some smaller arc bends connected so as to separate at the measurement station, because the probe holder (shown in Fig. 2) needs to be inserted at these points. The hind 90-deg bend is connected to the fore bend in rotation, that is, the curvature plane of the hind bend is perpendicular to that of the fore bend. The central curved axis of each bend is lying on the different curvature plane. In each bend the ratio of the curve radius to the tube radius is 6. The air flows through the tube; the inside tube radius denoted by a is 40.7 mm. There is a straight circular tube (8 m in length) at the start of the fore bend, having the same radius as that of the bend. The length of the straight tube is long enough so that the flow is fully developed before reaching the inlet to the bend.

An X-type hot wire probe is used to measure the velocities at the stations located at every $\pi/8$ turn of the bend. Figure 2 shows the probe positioned in the bend. The stem of the probe, 3 mm in diameter, is supported by the holder. Four needles, about 40 mm long, jut from the stem perpendicularly into the flow, and are equipped at their pointed ends with a pair of tungsten wires, 5 μm in diameter, which are at right angles to each other. Each wire must be placed at 45 degrees to the cross-section of the bend in order to measure the secondary flow velocity

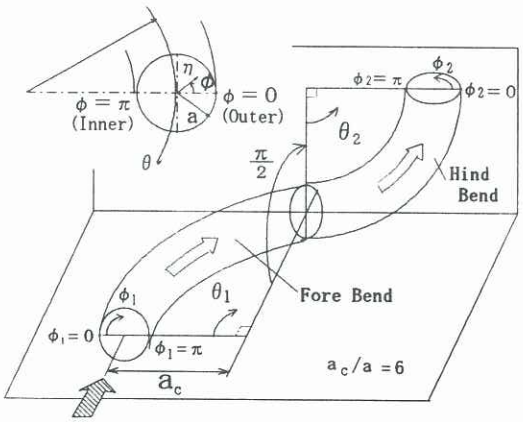

Fig. 1 Structure of Twisted S-Tube and Coordinates system

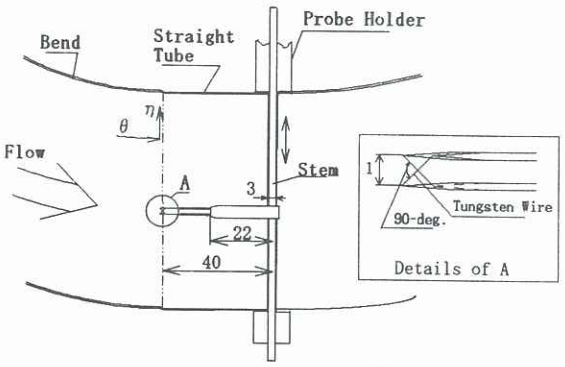

Fig. 2 Positioning of the Probe

components correctly. A short straight tube with a probe holder, which has the same diameter as the bend, is inserted between the small arc bends as a spacer so that the inclination of the wire is maintained properly.

The stem of the probe can be moved by a micrometer head along a radial line. In addition, the probe holder can be rotated circumferentially, so that there are twelve traverse radial lines, that is, at every circumferential angle $\pi/6$, in the circular cross-section.

The coordinate system used in this study is also shown in Fig. 1, where θ is the angle measured from the entrance of the bend, and η and ϕ are the radial and circumferential coordinates in the cross section, respectively. Subscripts 1,2 represent the coordinates for the fore bend and those for the hind bend, respectively. The radial line $\phi = 0$ is the outside of the curvature.

RESULTS AND DISCUSSION

Variation of time-mean axial flow velocity

Figure 3 (a) shows the variation of the profiles of dimensionless axial time-mean velocity $U_\theta (= u_\theta / u_m)$ along the diametric lines in the cross-sections at every $\pi/8$ turn through the twisted S-tube. u_θ and u_m are the axial velocity and the averaged velocity in the cross-section, respectively. Four profiles in the left half section of this figure are those for the fore bend along the diametric line, $\phi_1 = \pi/2, 3\pi/2$, which is perpendicular to the curvature plane of the bend depicted as the horizontal center line of this section. The leftmost profile describes the axisymmetric profile at the inlet of the fore bend. In the range $\pi/8 \le \theta_1 \le 3\pi/8$, measurements were made in the half cross-section of the bend only, because of the symmetry. In the right half section of the figure, five axial velocity profiles on the curvature plane, $\phi_2 = 0, \pi$, in the hind bend are shown. The plane, $\phi_2 = 0, \pi$ is continuous to the surface containing $\phi_1 = \pi/2, 3\pi/2$ in the fore bend.

The variation of the profiles on another continuous surface is shown in Fig. 3(b), which contains $\phi_1 = 0, \pi$ in the fore bend and $\phi_2 = \pi/2, 3\pi/2$ in the hind bend. The surface is perpendicular to that in Fig. (a).

By $3\pi/8$ into the fore bend the axial velocity decreases remarkably in the vicinity of the tube wall at the inside of the curvature($\phi_1 = \pi$) as shown in Fig. (b). The maximal axial velocity position shifts towards the outside of the curvature. At $\theta_2 = 0$ ($\theta_1 = \pi/2$) the velocity is larger

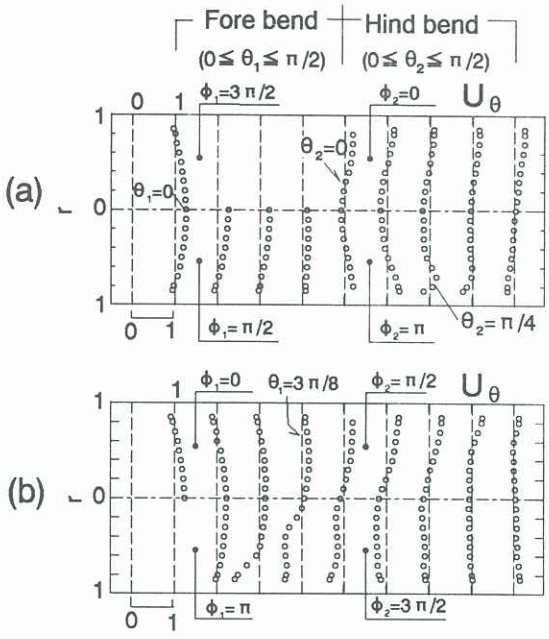

Fig. 3 Variation of the profiles of dimensionless axial time-mean velocity

at the outside of the curvature, while smaller at the inside, although the velocity on $\phi_1 = \pi$ is slightly increased more than that at $3\pi/8$. The profile is noted to be symmetric, as shown in Fig. (a), with respect to the central axis of the tube at $\theta_2 = 0$. This axial velocity development in the fore bent tube is closely related to the generation and progress in the secondary flow vortices induced by the centrifugal force due to the tube-axis curvature. These features of the velocity for the fore bend are similar to those for a single bend determined in the past several studies.

The axial velocity profile is changed by $\theta_2 = \pi/4$ in the hind bend. Especially, a part of the profile is distorted to be like a hook near the tube wall ($r \cong 0.7$) on $\phi_2 = \pi$ at $\theta_2 = \pi/4$, as a result, the axial velocity has a steep peak locally as shown in Fig. 3 (a). There is no symmetry plane for the axial velocity profile in this bend.

Contours of time-mean axial velocity and Secondary flow velocity vectors

Figure 4 (a)-(c) show the contours of dimensionless

time-mean axial velocity, U_θ, in the cross-section at three stations of the hind bend, $\theta_2 = 0, \theta_2 = \pi/4$ and $\theta_2 = \pi/2$, respectively. Figure 5 (a)-(c) show the vectors of the time-mean secondary flow velocity in the cross-section, which are divided by the averaged axial velocity to be nondimensionalized.

Because the curvature plane of the hind bend was perpendicular to that of the fore bend, the inflow velocity profile is not symmetrical with respect to the curvature plane, that is, the horizontal chord along $\phi_2 = \pi$ to $\phi_2 = 0$, as shown in Fig. 4 (a). The higher speed region exists in the upper half section at $\theta_2 = 0$. The region rotates clockwise downstream as shown in Fig. 4 (b) and (c). The rotation is definitely related to the secondary flow pattern drawn in Fig. 5 (b) and (c), which are regarded as almost one clockwise rotating vortex in those cross-sections. The vortex motion is generated because centrifugal force acting on the fluid toward the right is stronger in the upper cross-section than in the lower cross-section. This is because a higher speed region exits at the upper cross-section as mentioned about Fig. 4 (a).

Thus, the secondary flow pattern greatly differs in the hind bend from that in the fore bend. The maximal secondary flow velocity is about 30 % of the averaged axial velocity at $\theta_2 = \pi/4$. The profile of the axial velocity at $\theta_2 = \pi/2$ gets flatter than that at $\theta_2 = \pi/4$. The secondary flow keeps a right-handed rotation in this section, and the maximum is about 30% of the mean velocity, which is similar to that in the upper stream. Over a wide area in these cross-sections, the secondary flow is strengthened above than that at the inlet, $\theta_2 = 0$.

Correlations of fluctuating velocity and generation for tubulence intensity

The dimensionless rms values of fluctuating velocity correlation, $(\overline{u_\theta' u_\theta'})^{0.5}/u_m$ is shown in Fig. 6 as the contour map, and the correlation $\overline{u_r' u_\theta'}/u_m^2$ is shown in Fig. 7. At $\theta_2 = 0$, the rms value is low around the central portion of the upper half semicircular cross-section. Referring to Fig. 4 (a), the axial velocity is higher and the contours are sparser around this portion. The rms value is quite large around the central region in the cross-section, whose shape is similar to a horseshoe. Figure 4 (a) also shows that the velocity contours are denser in the horseshoe region.

By the $\pi/4$ turn of the hind bend, the contour profile of the rms value is largely deformed compared to that at the inlet. There is a great increase in the value near the tube wall around $\phi_2 = \pi$, as seen in Fig. 6 (b). On the other hand, the value is lower near the tube wall at the range of $0 < \phi_2 < \pi/2$. This means that the lower-value-region rotates clockwise from that at the inlet. This tendency is similar to that occurring in the case where the high speed region rotated as already shown in Fig. 4. At the outlet, $\theta_2 = \pi/2$, the contours are sparse over the wide area in the cross-section, although they remain rather dense near the tube wall at the range of $\pi/2 < \phi_2 < \pi$. The rms value is smaller in the region where the axial velocity is higher.

Figure 7 (b) shows that the contours for $\overline{u_r' u_\theta'}/u_m^2$ are much denser around the portion where the rms value is sharply increased in the cross-section at $\theta_2 = \pi/4$. They are sparser around the portion where the contours for the rms values are sparser. The distribution of $\overline{u_r' u_\theta'}/u_m^2$ affects the magnitude of the generation rate for the rms, hence it is found that the characteristic of the rms value is closely connected with its generation rate. The generation rate, *Ge*, can be calculated from the measurement data at each cross-section by the following definition, which is shown in Fig. 8 as a contour map.

$$Ge = -4\left[R_{r\theta}\frac{\partial U_\theta}{\partial r} + \frac{R_{\phi\theta}}{r}\frac{\partial U_\theta}{\partial \phi} + \frac{R_{\theta\theta}}{h_\theta}\left(\frac{\partial U_\theta}{\partial \theta} + U_r\cos\phi - U_\phi\sin\phi\right)\right],$$

where

$R_{r\theta} = \overline{u_r' u_\theta'}/u_m^2$, $R_{\phi\theta} = \overline{u_\phi' u_\theta'}/u_m^2$, $R_{\theta\theta} = \overline{u_\theta' u_\theta'}/u_m^2$,

$h_\theta = a_c/a + r\cos\phi$, $r = \eta/a$.

CONCLUSION

(1) The higher speed region away from the curvature plane at the inlet of the hind bend rotates toward the outer side of the curvature downstream. Axial velocity is fairly homogenized at the outlet cross-section of the hind bend except near the wall region.

(2) A pair of symmetrical vortices generated in the fore bend develops to change into an almost one directional rotating vortex in the hind bend of twisted S-tube. The maximal secondary flow velocity reaches about 30 % of the averaged axial velocity in the hind bend.

(3) The magnitude of r.m.s value for the correlation of the axial fluctuating velocities increases largely near the wall on the inner side of the curvature by the $\pi/4$ turn of the hind bend. The turbulence generation rate for the correlation also becomes quite large in the same region, so it is proved to be closely connected with the correlation.

REFERRENCES

Aoyama, Y., Hijikata K. and Futagami K., 1990, "Secondary Motion and Turbulence of the Flow through a circular π -curved bent Tube and a S-duct", Trans. JSME 56-531, pp. 3321-3327 (in Japanese).

Akiyama, M., Murakoshi, T., Sugiyama, H., Cheng, K.C. and Nishiwaki, I., 1988, "Numerical Solution of Convective Heat Transfer for Reverse Transition in the Bend Tube by a Low-Reynolds-Number Turbulent Model," JSME International Journal, Vol. 31, No. 2, pp. 289-298.

Azzola, J., Humphrey, J.A.C., Iacovides, H. and Launder, B.E., 1986, "Developing Turbulent Flow in a U-Bend of Circular Cross-Section: Measurement and Computation," Trans. of ASME, Vol 108, pp. 214-221.

Baughn J.W., Iacovides, H., Jackson, D.C. and Launder, B.E., 1987, "Local Heat Transfer Measurements in Turbulent Flow Around a 180-deg Pipe Bend," Trans. of ASME, J. of Heat Transfer, vol. 109, pp.43-48.

Enayet, M.M., Gibson, M.M., Taylor, A.M.K.P. and Yianneskis, M., 1982, NASA Contract rep., 3551.

Iacovides, H. and Launder B.E., 1984, "The Computation of Momentum and Heat Transport in Turbulent Flow around Pipe Bends," Proc. 1st UK National Heat Transfer Conference, vol.2, I. Cheme. Engrs. Symposium Series 86, pp.1097-1114.

Rowe, M., 1970, "Measurements and Computations of Flow in Pipe Bends," J. Fluids Mech., Vol. 43, pp.771-783.

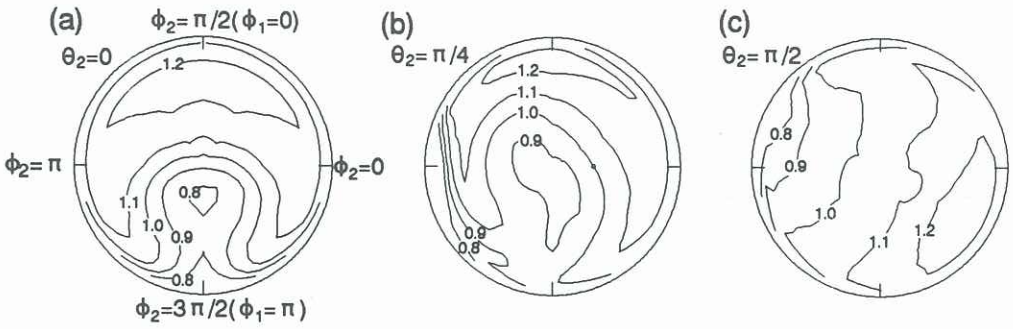

Fig. 4 Contours of dimensionless time-mean axial velocity ($Re=2\times10^4$)

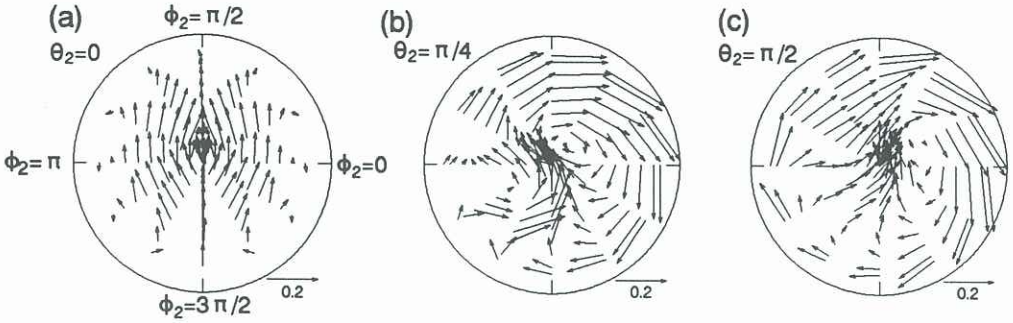

Fig. 5 Dimensionless secondary flow velocity vectors ($Re=2\times10^4$)

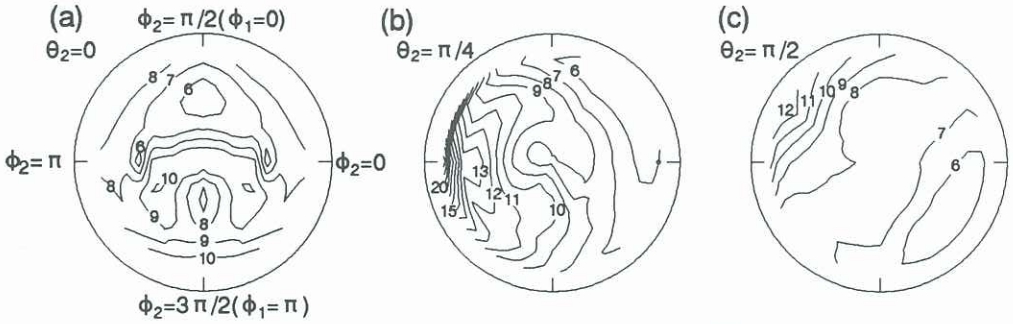

Fig. 6 Contours of r.m.s. values of fluctuating velocity correlation, $(\overline{u_\theta' u_\theta'})^{0.5}/u_m\times10^2$, ($Re=2\times10^4$)

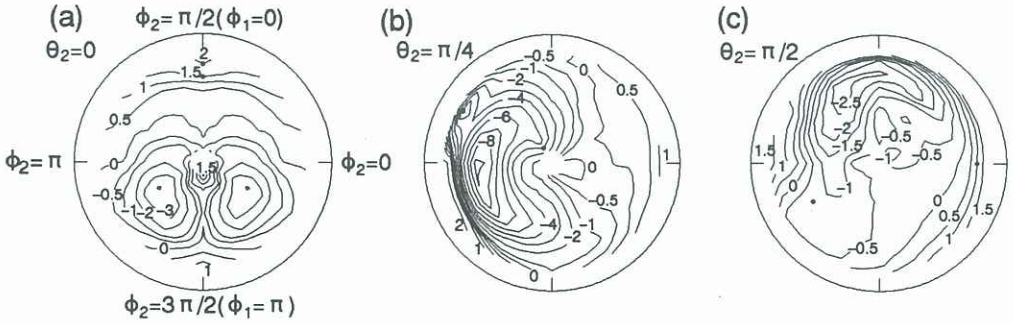

Fig. 7 Contours of dimensionless fluctuating velocity correlation, $\overline{(u_r' u_\theta')}/u_m^2\times10^3$, ($Re=2\times10^4$)

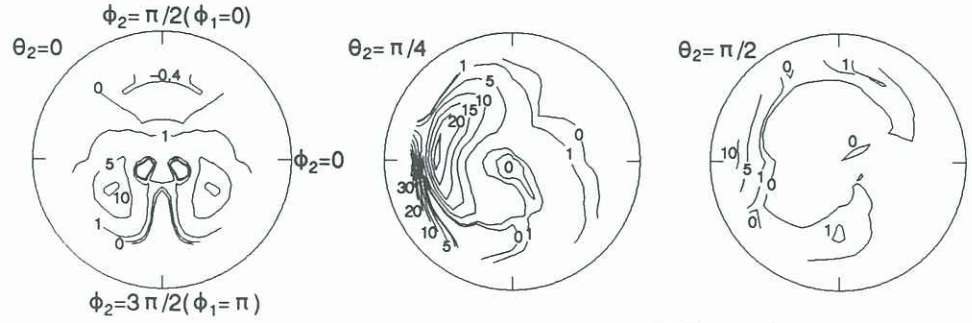

Fig. 8 Contours of dimensionless generation for $\overline{u_\theta' u_\theta'}$, ($\times10^3$)